Boundary-Layer Meteorology (2005) 116: 423–443
DOI 10.1007/s10546-004-7956-x

A SIMPLE ENERGY BALANCE MODEL FOR REGULAR BUILDING ARRAYS

M. KANDA*, T. KAWAI, M. KANEGA, R. MORIWAKI, K. NARITA[1] and A. HAGISHIMA[2]

Department of International Development Engineering, Tokyo Institute of Technology, 2-12-1 O-okayama, Meguro-ku, Tokyo, 152-8552 Japan; [1]Department of Engineering, Nippon Institute of Technology, Japan; [2]Interdisciplinary Graduate School of Engineering Sciences, Kyushu University, Japan

(Received in final form 18 November 2004)

Abstract. A *s*imple *u*rban energy balance *m*odel for *m*esoscale simulations (SUMM) was tested using results from an outdoor scale-model experiment. The model geometry is assumed to be an infinitely extended regular array of uniform buildings, each of which is composed of six faces (roof, floor, and four vertical walls). The SUMM explicitly considers the three dimensionality of surface geometry and theoretically predicts the energy balance at each face without time-consuming iterations. The SUMM was compared with outdoor scale-model experiments. The simulated energy balance and surface temperatures agree well with the values measured on a reduced-scale hardware model corresponding to the numerical model geometry.

Keywords: Bulk transfer coefficient, Energy balance, Outdoor experiment, Regular building array, Theoretical model, Urban canopy.

1. Introduction

Urban surface geometry has a large, but complex, influence on urban meteorology. Unfortunately, explicit inclusion of buildings into weather simulations using computational fluid dynamic methods is quite time consuming and thus is still unrealistic for practical applications. An alternative approach has been to develop simple urban energy balance models for use in mesoscale simulations (Arnfield, 1982; Masson, 2000; Kusaka et al., 2001; Martilli et al., 2002; Sailor and Fan, 2002). These models generally assume two-dimensional (2-D) infinite street canyons mainly because it allows one to treat radiation with analytic theory. To overcome the restriction of a 2-D radiation scheme, we have recently developed a simple theoretical radiation scheme applicable for three-dimensional (3-D) rectangular obstacles arrays (Kanda et al., 2005).

* E-mail: kanda@ide.titech.ac.jp

In this paper, we propose a new *s*imple *u*rban energy balance *m*odel for *m*esoscale simulations (SUMM). The SUMM consists of a 3-D theoretical radiation scheme (Kanda et al., 2005) and the conventional heat transfer expression that uses a network of resistances (Masson, 2000; Kusaka et al., 2001). The present model allows one to readily calculate the energy balance and surface temperature at each face of the urban canopy (i.e., roof, floor, and four vertical walls) without time-consuming iterations.

We also performed outdoor experiments using a reduced-scale hardware model that corresponds to the numerical model geometry. The purpose of the experiments was twofold. The first is to determine unknown physical parameters such as the local bulk transfer coefficient and the reflective properties at each face. The values of the local bulk transfer coefficient, which is a key parameter in turbulent transport, are poorly known (Barlow and Belcher, 2002; Narita, 2003; Hagishima et al., 2005). The other purpose is to evaluate the performance of the present numerical model. Generally, the geometrical gap between real cities and modelled urban canopies is too large to directly evaluate the model performance, so that miniature scale-model experiments can be an effective tool in evaluating numerical models (Kanda, 2005).

2. Theoretical Scheme

2.1. Urban canopy model

The urban canopy geometry employed in this study is illustrated in Figure 1. In this model, streets and buildings are represented by an infinitely extended regular array of buildings with a square horizontal cross-section and uniform surface properties. So long as uniform building arrays are used, the surface geometry can be characterised by only two geometrical parameters: the plane area index λ_p and the frontal area index λ_f, defined as

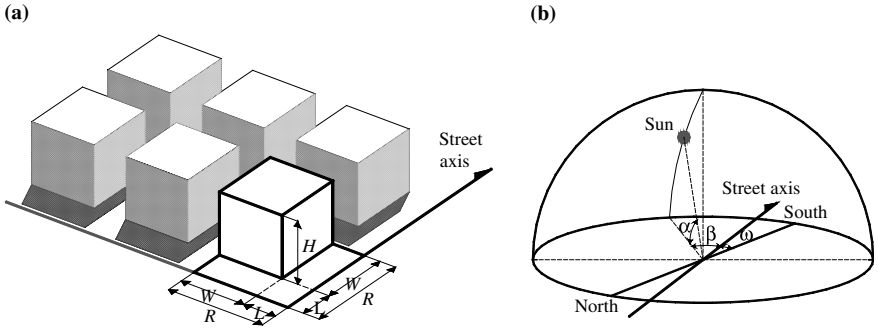

Figure 1. Urban canopy geometry employed in this study. (a) Building dimensions. (b) Orientation of the streets with respect to the sun and north–south.

$$\lambda_p = W^2/(W+L)^2, \tag{1}$$

$$\lambda_f = WH/(W+L)^2, \tag{2}$$

where W and H are the horizontal dimension and height of the buildings, respectively, and L is the width of the streets. The main axis of the canopy is defined to be parallel to the street and oriented at an azimuthal angle ω from north–south measured counter-clockwise as viewed from above. The solar elevation angle is α, and the solar azimuthal angle measured from the street axis is β. The model is applicable to any time and location. The energy balance and surface temperature are predicted at each face, and the resulting total energy balance is required to be closed over the surface layer.

2.2. Shortwave radiation budget with multi-reflections

We described the details of the 3-D radiation scheme employed in the present model (Kanda et al., 2005) so that only the outline of the scheme is reviewed here. It is assumed that all faces are Lambertian and thus the reflected radiations are isotropic. Mirror reflection of direct shortwave radiation does not occur. Under the above assumptions, the multi-reflective exchange of shortwave is straightforward once the view factors and sunlit-shadow distributions are known.

The absorbed and reflected radiative energy per unit area of each face at the first reflection, $S_{ab}(i,1)$ and $S_{ref}(i,1)$, can be written

$$S_{ab}(i,1) = (1-a(i))S(i) + (1-b(i))S_{dif}V(i,\mathrm{sky}), \tag{3}$$

$$S_{ref}(i,1) = a(i)S(i) + b(i)S_{dif}V(i,\mathrm{sky}), \tag{4}$$

where i is the face number from 1 to 6 corresponding to the four walls, the floor, and the roof; $S(i)$ is the direct shortwave radiative energy reaching the unit area of face i, $V(i,\mathrm{sky})$ is sky view factor from face i; S_{dif} is the diffuse shortwave radiative energy from the sky, and $a(i)$ and $b(i)$ are the albedos of direct and diffuse shortwave radiation, respectively. The theoretical treatment of sunlit-shadow distribution ($S(i)$) and view factor ($V(i,\mathrm{sky})$) follows the theoretical scheme described in Kanda et al. (2005). After the first reflection, isotropic components in the multi-reflection processes remain but no direct component exists. The absorbed and reflected radiative energy per unit area of each face at the Nth reflection is calculated as the sum of the $N-1$th reflected beam from the other faces as

$$S_{ab}(i,N) = (1-b(i))\sum_{j=1}^{6} S_{ref}(j,N-1)V(j,i), \tag{5}$$

$$S_{\mathrm{ref}}(i,N) = b(i)\sum_{j=1}^{6} S_{\mathrm{ref}}(j,N-1)V(j,i), \tag{6}$$

where $V(i,j)$ is the view factor from face i to face j. The total absorption and reflection of shortwave per unit area of each face after $N_{\max}$ multi-reflections, $ST_{\mathrm{ab}}(i)$ and $ST_{\mathrm{ref}}(i)$ are

$$ST_{\mathrm{ab}}(i) = \sum_{N=1}^{N_{\max}} S_{\mathrm{ab}}(i,N), \tag{7}$$

$$ST_{\mathrm{ref}}(i) = \sum_{N=1}^{N_{\max}} S_{\mathrm{ref}}(i,N). \tag{8}$$

The resulting upward shortwave radiation from unit lot area to the sky, $S^{\uparrow}$ is

$$S^{\uparrow} = \left[S^{\downarrow}A_{\mathrm{lot}} - \sum_{i=1}^{6} ST_{\mathrm{ab}}(i)A(i)\right] \Big/ A_{\mathrm{lot}} = \left[\sum_{i=1}^{6} ST_{\mathrm{ref}}(i)V(i,\mathrm{sky})A(i)\right] \Big/ A_{\mathrm{lot}}, \tag{9}$$

where $S^{\downarrow}$ is the downward shortwave radiation to unit lot area, $A(i)$ are the area of the face i; $A_{\mathrm{lot}} = (L+W)^2 = R^2$.

2.3. Longwave radiation budget with multi-reflections

Due to the nature of non-directional incident longwave radiation, the algorithm for solving the longwave radiation budget is essentially the same as that for the diffuse shortwave radiation except the treatment of the emission from the wall that is directly related to the wall temperature. The absorbed and reflected longwave energy per unit area of each face at the first reflection, $L_{\mathrm{ab}}(i,1)$ and $L_{\mathrm{ref}}(i,1)$ are written

$$L_{\mathrm{ab}}(i,1) = \quad \varepsilon(i)L^{\downarrow}V(i,\mathrm{sky}) - \sigma\varepsilon(i)T_{\mathrm{S}}(i)^4, \tag{10}$$

$$L_{\mathrm{ref}}(i,1) = (1-\varepsilon(i))L^{\downarrow}V(i,\mathrm{sky}) + \sigma\varepsilon(i)T_{\mathrm{S}}(i)^4, \tag{11}$$

where $L^{\downarrow}$ is the longwave radiation from the sky, $\varepsilon(i)$ is the emissivity, σ is the Stefan–Boltzmann constant, and $T_{\mathrm{S}}(i)$ is the surface temperature. The absorbed and reflected radiative energy per unit area of each face at the Nth reflection, $L_{\mathrm{ab}}(i,N)$ and $L_{\mathrm{ref}}(i,N)$, are calculated as the sum of the $N-1$th reflected beams from the other faces

$$L_{\mathrm{ab}}(i,N) = \sum_{j=1}^{6} \varepsilon(i)L_{\mathrm{ref}}(j,N-1)V(j,i), \tag{12}$$

$$L_{\mathrm{ref}}(i,N) = \sum_{j=1}^{6} (1-\varepsilon(i)) L_{\mathrm{ref}}(j,N-1) V(j,i). \tag{13}$$

The total absorption and reflection of longwave radiation per unit area of each face after $N_{\max}$ multi-reflections, $LT_{\mathrm{ab}}(i)$ and $LT_{\mathrm{ref}}(i)$, are

$$LT_{\mathrm{ab}}(i) = \sum_{N=1}^{N_{\max}} L_{\mathrm{ab}}(i,N), \tag{14}$$

$$LT_{\mathrm{ref}}(i) = \sum_{N=1}^{N_{\max}} L_{\mathrm{ref}}(i,N). \tag{15}$$

The resulting upward longwave radiation from unit lot area to the sky, $L^{\uparrow}$, is calculated as

$$L^{\uparrow} = \left[L^{\downarrow} A_{\mathrm{lot}} - \sum_{i=1}^{6} LT_{\mathrm{ab}}(i) A(i) \right] \Big/ A_{\mathrm{lot}} = \left[\sum_{i=1}^{6} LT_{\mathrm{ref}}(i) V(i,\mathrm{sky}) A(i) \right] \Big/ A_{\mathrm{lot}}. \tag{16}$$

The radiative temperature is a representative temperature of the urban surface (Voogt and Oke, 1997), and can be defined as

$$T_{\mathrm{R}} = (L^{\uparrow}/\sigma)^{0.25}. \tag{17}$$

2.4. Sensible heat fluxes

To treat the sensible heat flux, we use the conventional heat transfer expression involving a network of resistances (Masson, 2000; Kusaka et al., 2001). The local sensible heat flux $H(i)$ from the face i to the sky (Figure 2a) is

$$H(i) = c_p \rho C_H(i) U_{\mathrm{a}} (T_{\mathrm{S}}(i) - T_{\mathrm{a}}), \tag{18}$$

where c_p is the specific heat, ρ is the air density; U_{a} and T_{a} are the wind speed and air temperature at a reference height z_{a} in the surface layer, respectively; and $C_H(i)$ is the local bulk transfer coefficient between the face i and the reference height. $C_H(i)$ is equivalent to the inverse of the resistance. The total sensible heat flux from unit lot area to the sky H is

$$H = \left[\sum_{i=1}^{6} H(i) A(i) \right] \Big/ A_{\mathrm{lot}}. \tag{19}$$

If we relate the network resistance expression (Figure 2a) with a slab-type formulation (Figure 2b), then the total sensible heat flux (H) in Equation (19) can be rewritten as

$$H = c_p \rho C_H U_{\mathrm{a}} (T_H - T_{\mathrm{a}}), \tag{20}$$

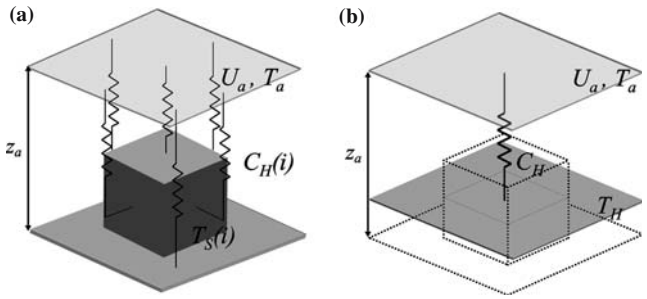

Figure 2. Structure of the computational model. (a) Network-resistance model. (b) Slab-model.

where C_H and T_H are the 'surface-layer' bulk transfer coefficient and effective surface temperature, respectively. From the identical equation in terms of T_a produced by Equations (18), (19), and (20), C_H and T_H can be described as,

$$C_H = \left[\sum_{i=1}^{6} C_H(i)A(i)\right] \Big/ A_{\mathrm{lot}}, \tag{21}$$

$$T_H = \left[\sum_{i=1}^{6} T_S(i)C_H(i)A(i)\right] \Big/ C_H A_{\mathrm{lot}}. \tag{22}$$

Equation (22) suggests that the 'effective surface temperature', an alternative representation of urban surface temperature, can be derived from the average of the surface temperatures weighted by the local bulk transfer coefficient times the area. Equations (17) and (22) show that the radiative and effective surface temperatures are different.

The problem is how to parameterise the local bulk transfer coefficients $C_H(i)$. The common way is to adopt a wall function such as the Monin–Obukhov Similarity (MOS) relationship. However, the MOS is only valid for the 'integrated' heat transfer from the canopy layer to the surface layer (C_H), and the application to the 'local' heat transfer within the canyon ($C_H(i)$) is physically incorrect. For this reason, the estimation of $C_H(i)$ has been a general problem in simple energy balance models (Barlow and Belcher, 2002; Narita, 2003; Barlow et al., 2004; Hagishima et al., 2005). Here we adopt the following two-step approach. First, C_H for the surface layer is theoretically predicted using the MOS (e.g. Garratt, 1992) as

$$C_H = \frac{\kappa^2}{\left(\int_{z_0/L}^{(z_a-z_d)/L} \Phi_M(\varsigma)\frac{d\varsigma}{\varsigma}\right)\left(\int_{z_{0T}/L}^{(z_a-z_d)/L} \Phi_H(\varsigma)\frac{d\varsigma}{\varsigma}\right)}, \tag{23}$$

where κ is the von Karman constant, L is Obukhov length scale, ζ is a non-dimensional height $(= (z - z_d)/L)$, $\Phi_M(\zeta)$ and $\Phi_H(\zeta)$ are the universal

functions for momentum and heat, respectively, and z_0, z_{0T} and z_d are the roughness lengths for momentum and for heat, and the displacement height, respectively. The momentum parameters z_0 and z_d can be semi-theoretically predicted from the geometric parameters λ_p and λ_f using Macdonald et al.'s formulation (1998), although this kind of formulation involves uncertainties in the application for real urban fields (Grimmond and Oke, 1999). The roughness length for heat z_{0T} can be determined from z_0 if the ratio z_0/z_{0T} is known. Although $\ln(z_0/z_{0T})$ for rough walls is typically 2.0 (Garratt and Francey, 1978), the values in urban areas are relatively large (Voogt and Grimmond, 2000). We use a typical value in a residential area of Tokyo (Kanda and Moriwaki, 2002; Moriwaki and Kanda, 2003), which is

$$\ln(z_0/z_{0T}) = 6.0. \tag{24}$$

This relationship was derived from the ensemble average of one-year continuous turbulent data from a tower. It should be noted that z_{0T} values in urban areas show large scatter and the assumption here is not robust. Once C_H is known from Equations (23) and (24), then we can distribute C_H to the individual values of $C_H(i)$, provided that the relative values of $C_H(i)$ normalised by$C_H(i = 6; \text{roof})$ are known from the available dataset (Barlow and Belcher, 2002; Narita, 2003, 2004). To strengthen the relatively poor dataset of relative values of $C_H(i)$, we used a new method to measure local bulk transfer coefficient using outdoor scale-model experiments. Details of this method can be found in Section 3.2.

The treatment of latent heat flux $LE(i)$ follows the same framework as that of the sensible heat flux:

$$LE(i) = l\rho B(i) C_H(i) U_a(q_s(i) - q_a), \tag{25}$$

where l is the latent heat of vaporisation, $B(i)$ is the wetness parameter for surface i, q_a is the specific humidity at the reference height z_a, and $q_s(i)$ is the saturated specific humidity for the surface temperature. $B(i)$ can range from 0 (completely dry) to 1.0 (completely wet), depending on the vegetation or the water availability at face i.

2.5. Surface temperatures

The energy balance equation for each face i is

$$Rn(i) - H(i) - LE(i) = G(i), \tag{26}$$

where $Rn(i)$ is the net radiation ($= ST_{ab}(i) + LT_{ab}(i)$), and $G(i)$ is the conductive heat flux into the solid materials. The temperature profiles inside the walls, floor, and roof are solved using the following one-dimensional energy conservation equation with a variable grid interval:

$$\frac{\partial T_{\mathrm{in}}(i)}{\partial z} = \frac{1}{\rho(i)c(i)}\left(\lambda(i)\frac{\partial^2 T_{\mathrm{in}}(i)}{\partial z^2}\right), \tag{27}$$

where $\lambda(i)$ and $\rho(i)c(i)$ are the interior thermal conductivity and volumetric heat capacity for surface i. The surface boundary condition of Equation (27) is given from the surface energy balance, Equation (26). Although the internal boundary condition of Equation (27) should be predicted by coupling the indoor energy balance model, it is tentatively assumed to either be the zero heat flux or prescribed from the observed temperature value. The total conductive heat flux stored in unit lot area G is calculated from

$$G = \left[\sum_{i=1}^{6} G(i)A(i)\right] \Big/ A_{\mathrm{lot}}. \tag{28}$$

3. Outdoor Experiment

3.1. Model set-up

To test the numerical model, we performed outdoor experiments using a 1/50 reduced-scale hardware model; the site was located in Matsusaka, Mie prefecture, Japan (34°34′N, 136°32′E). Flat terrain and bare soil or short grasses extended at least 10 km in all directions. The model surface geometry consisted of cubic concrete blocks $H = 0.15$ m on a side, regularly distributed on flat concrete plates with a total area of 12×9 m^2 (Figure 3); the plane aspect ratio of the model was $\lambda_{\mathrm{p}} = 0.25$. The long axis is roughly north-west, the dominant wind direction at the site. To capture a sufficiently developed internal boundary layer (IBL), all sensors were installed 10 m downstream from the leading edge (Figure 3). We judged from the observed vertical

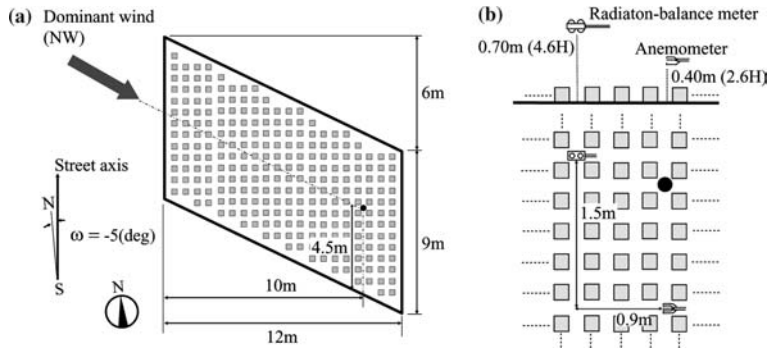

Figure 3. Schematic of the outdoor hardware-scale model: (a) Array of blocks and location of sensors (black dot). (b) Configuration of sensors.

temperature profiles (measured using thermocouples) that the IBL depth ranged from $2.6H$ to $4.0H$ at the distance of the sensors. Upward and downward shortwave and longwave radiation fluxes were measured separately using a radiation-balance meter (Eiko MR-40) at 0.7 m above the ground ($z = 4.6H$). A compact sonic anemometer (Kaijo-WA590) with 0.05-m sensor length was installed 0.40 m above the ground ($z = 2.6H$); it was not used for the sensible heat estimation but only for the mean velocity measurements. To accurately close the energy balance, the conductive heat fluxes at each surface $G(i)$ need to be measured, mainly because the energy balance residual (net radiation minus the turbulent fluxes) cannot be used in place of the conductive flux measurements, due to the energy imbalance problem with the eddy covariance method (e.g. Kanda et al., 2004a). The measurement of $G(i)$ was made possible by using very thin heat plates (Captec HF-300, 0.4 mm thick) and carefully coating them with the same material as the obstacles. The sensible heat flux of individual surfaces $H(i)$ was estimated from the energy balance residual of $Rn(i) - G(i)$, where $G(i)$ was directly measured using heat plates and $Rn(i)$ was estimated using a high-accuracy radiation scheme with measured$L^{\downarrow}$, $S^{\downarrow}$, and $T_S(i)$ (Voogt and Oke, 1990; Kanda et al., 2005). The surface temperatures $T_S(i)$ were measured at multiple points using 0.2-mm thermocouples (Figure 4). All measurements were stored once per second and averaged for 10 min using a Campbell Scientific CR-23X datalogger. All the data selected for the present analysis were obtained under sufficiently dry conditions so as to ignore the latent heat flux contribution ($LE(i)$).We previously found that $LE(i)$ was negligible five days after rainfall (Moriwaki and Kanda, 2003).

3.2. Estimate of the local bulk transfer coefficient

Apart from the numerical model procedure mentioned above, we used a new method to measure the local bulk transfer coefficient ($C_H(i)$) using outdoor scale-model experiments. From Equations (18) and (26), $C_H(i)$ can be described as

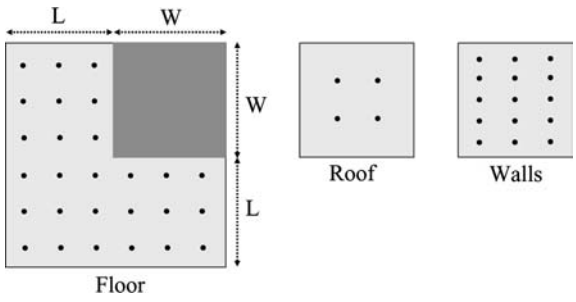

Figure 4. The alignment of thermocouples (dots).

$$C_H(i) = (Rn(i) - G(i))/(c_p \rho U_a (T_S(i) - T_a)). \quad (29)$$

Fortunately, $G(i)$ is directly measured, and $Rn(i)$ can be estimated using a high-accuracy radiation scheme with measured $L^{\downarrow}$, $S^{\downarrow}$, and $T_S(i)$ (Voogt and Oke, 1990; Kanda et al., 2005). Thus, $C_H(i)$ is calculated using the measured T_a and U_a. Using a similar method, Swaid (1993) estimated the local bulk transfer coefficients of a set of parallel polystyrene plates of a 2-D street canyon, and could ignore the heat storage term because the walls were very thin. In addition to the 3-D cube array shown in Figure 3, we performed an experiment that approximates a 2-D street canyon to compare with previously published indoor experimental data. The 2-D canyon was composed of the same concrete blocks with street width equal to the block height; there is a constant north-west wind at night at the experimental site, giving a near-neutral condition. Thus, only the nocturnal dataset is used for the ensemble average of $C_H(i)$. The experimental conditions and thresholds of selecting data for this analysis are listed in Table I and Table II, respectively. According to the review of Hagishima et al. (2005) the 'absolute' values of local bulk transfer coefficients vary considerably from site to site and are currently difficult to determine through a simple formulation. Therefore, we focus on the 'relative' values of the individual local bulk transfer coefficient. The estimated $C_H(i)$ normalised by the value for the roof surface is compared with the two indoor experiments in Figure 5. Barlow et al. (2004) used a naphthalene sublimation technique to determine local bulk transfer

TABLE I

Experimental conditions.

	Experiment period	Time period used for this analysis	Integration time of a sample (min)	The number of selected samples
3D	25 October to 25 December, 2003	0000 to 0600	10	140
2D	2 February to 21 March, 2004	0000 to 0600	10	50

TABLE II

Thresholds for selecting samples.

Reference wind speed U_a (m s^{-1})	The range of wind direction (deg)	Temperature difference $T_S(i) - T_a = \Delta T$ (K)	Stability range $Rb = \frac{gH}{(T_a+273)} \frac{(T_a - T_C^*)}{U_a^2}$
$U_a > 1.0$	270–360	$\lvert\Delta T\rvert > 0.5$	$\lvert Rb\rvert < 0.025$

*T_C: complete surface temperature, Thresholds of selecting data. $T_C = \left[\sum_{i=1}^{6} T_S(i) A(i)\right] \Big/ A_{lot}$.

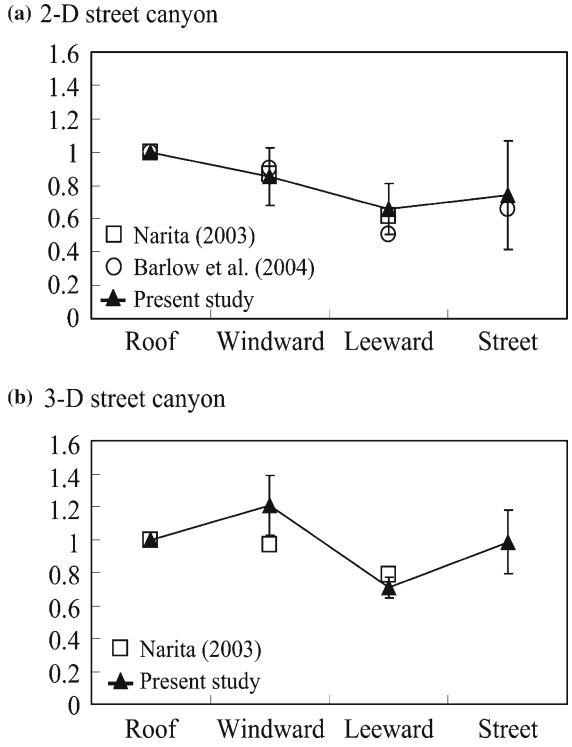

Figure 5. Local bulk transfer coefficients normalised by the value for the roof. (a) 2-D-street canyon with height/street ratio equal to 1.0. (b) 3-D-street canyon with $\lambda_p = 0.25$. The Barlow et al. (2004) experiments used the naphthalene sublimation method and the Narita (2003) experiments used the evaporation method. Leeward and windward values for 3-D street canyon were average for two surfaces; north-west and south-east, respectively. The error bars indicate the run-to-run variability for the present experiments.

coefficients of various 2-D canyons. Narita (2003) measured the evaporation rate of saturated filter paper pasted to the surfaces of 3-D and 2-D model canopies to study the local bulk transfer coefficient. The present results both for the 2-D and 3-D street canyons agree well with the indoor experiments, even though the present outdoor experiments estimated the local bulk transfer coefficient for heat instead of mass transfer that was relevant to the indoor experiments.

3.3. Similarity requirements

Scale modelling requires dynamical and geometrical similarity to the real world. Dynamical requirements include (1) radiation similarity, (2) flow similarity, and (3) thermal inertia similarity (Kanda, 2005).

As long as real urban materials are used and real boundary conditions are given, the similarity of radiation is always acceptable because the linear dimensions of any scale model are much larger than the relevant radiation wavelengths.

For neutrally stratified flows, Reynolds number independence is required in terms of the normalised Navier–Stokes equation. The 'critical' Reynolds numbers, above which the characteristics of turbulent flow around obstacles are independent of the Reynolds number, have been studied in wind tunnels (e.g., Castro and Robins, 1977; Uehara et al., 2003). Generally, the Reynolds number (Re) for a building is based on the building's height and the wind speed at that height in the undisturbed flow. The critical value of Re is several thousand, and the building Reynolds number in the present experiments are about 10^4, and thus slightly larger than the critical values.

Obtaining similarity of thermal inertia is the most problematic. Thermal admittance, which equals the square root of the product of the body's thermal conductivity and volumetric heat capacity, should be the same in the model as for real urban materials. Unfortunately, this is very difficult to scale, and the present experiments do not satisfy this requirement.

4. Numerical Simulation

4.1. Experimental dataset used in the evaluation of SUMM

As mentioned in Section 3.3, the thermal inertia and energy balance of the present hardware model are not typical of real world conditions. Therefore, we do not make quantitative comparisons between the measured surface energy balance and data from real cities. Nevertheless, it is important to evaluate the numerical model (SUMM) with a comprehensive experimental dataset. There are two reasons for this: (1) In the field, the acquisition of a comprehensive dataset involving all energy balance components and surface temperature at each constituent surface is very difficult and limited (e.g. Rotach, 2002), and (2) once the numerical model (SUMM) is successfully validated for the reduced scale, it is straightforward to apply the SUMM to the real scale by adjusting the volumetric heat capacities.

The estimated parameters of the experimental model are summarised in Table III. The experimental period was three months, although the appropriate dataset, for which the latent heat flux was negligible and the percentage of sunshine exceeded 80% in the daytime, was found to be only for 5 days. In the available 5-day dataset, all days had similar tendencies, and thus the simulation results for only one day are shown below.

TABLE III
Estimated parameters of the experimental model.

Experiment period		25 October to 25 December, 2003
The number of appropriate days for the validation[a]		5
The date used for the simulation		30 October, 2003
Inclination of street axis (in Figure 3)		−5 (deg)
Facet albedo of direct shortwave (in Section 2.2)	$a(i)$	Empirical function of incident angle γ_i[b]
Facet albedo of diffusive shortwave (in Section 2.2)	$b(i)$	$2\int_0^{\pi/2} a(i)\cos\gamma_i \sin\gamma_i d\gamma_i$
Diffuse/direct ratio of shortwave radiation		0.25
Emissivity of the concrete	ε	0.98
Volumetric heat capacity of the concrete	ρc	2.48×10^6 (J m^{-3} K)
Thermal conductivity of the concrete	λ	0.50 (W m^{-1} K^{-1})

[a] The latent heat flux was negligible and the percentage of sunshine exceeded 80%.
[b] $a(i) = f(\gamma_i) = 0.519282 - 0.329635\cos\gamma_i + 0.309507 \times (\cos\gamma_i)^2 - 0.122024 \times (\cos\gamma_i)^3$, where γ_i is the solar incident angle defined differently for the individual surfaces.

4.2. Computational procedure

The geometrical parameters, thermal properties and reflectivity of the SUMM were set to be the same as those of the outdoor experiments (Table II and Table III). The thermal conductivity and volumetric heat capacity of the concrete cubes were precisely measured indoors. The emissivity and the albedo in terms of the incident solar angle were regressed from preliminary outdoor experiments on the flat basement without cubes (Kanda et al., 2005). The diffuse/direct ratio of the incident shortwave radiation fluxes was assumed to be 1:4. The ray paths were followed for five reflections. The outer boundary conditions including the downward shortwave and longwave radiation fluxes $S\downarrow$ and $L\downarrow$, air temperature T_a and wind speed U_a at $z = 0.4$ m, and the inner boundary conditions of the core temperatures of a cube and a plate at the depth of 0.075 m, were given from the measured values for every 1-min period.

5. Results and Discussion

5.1. Energy balance of the constituent surfaces

The simulated energy balance components ($Rn(i)$, $H(i)$ and $G(i)$) and surface temperature ($T_S(i)$) of six constituent surfaces are compared with the

observed counterparts (Figures 6–9). The simulated energy balance components generally follow the observed diurnal trends, although they have locally some quantitative disagreement.

Particularly, the simulated net radiation agreed fairly well with the observed values (Figure 6). The observed $Rn(i)$ may include some errors, since they were not directly measured but were estimated from a high-accurate radiation model with the observed incoming radiation fluxes and surface temperatures. Voogt and Oke (1990) measured longwave fluxes at different points in a single canyon and reported that the accuracy of the radiation model of Arnfield (1982) was $\pm 1\%$. Kanda et al. (2005) reported that the high-accurate model can predict the observed shortwave fluxes to within $\pm 10\%$ accuracy. Thus the observed $Rn(i)$ could have, at most, a $\pm$ 10% error.

The simulated sensible heat fluxes underestimate the observed values especially in the morning (Figure 7). One possible reason for this is that the

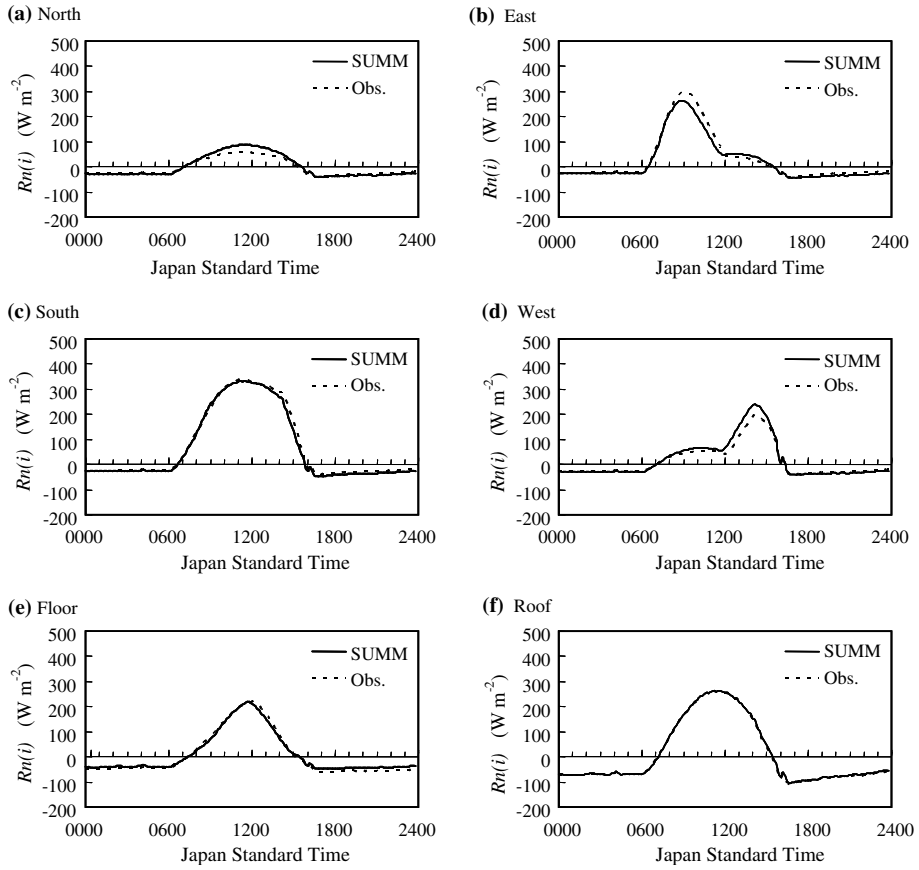

Figure 6. Net radiation in the simulations (bold lines) and measurements (dotted lines). Positions are (a) north wall, (b) east wall, (c) south wall, (d) west wall, (e) floor and (f) roof.

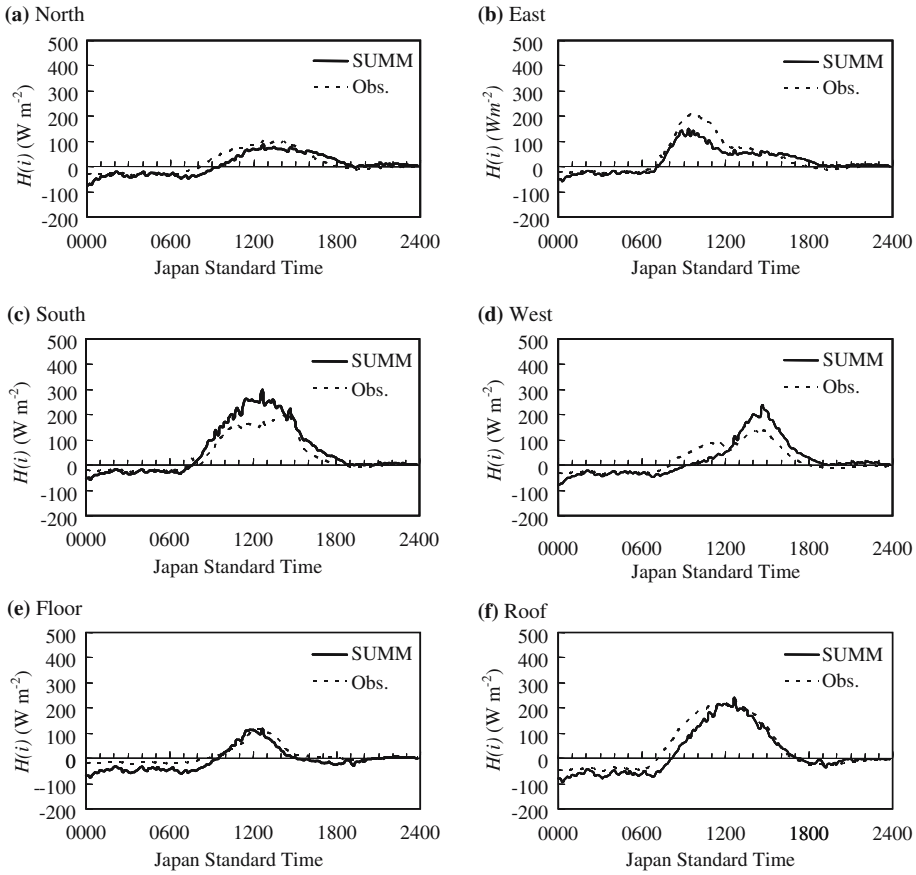

Figure 7. Sensible heat flux in the simulations (bold lines) and measurements (dotted lines).

current local bulk transfer coefficients $C_H(i)$ were derived from neutrally-stratified conditions (Section 3.2) and thus they do not consider the influence of local atmospheric stability. Generally in the morning, surface temperature increases more rapidly and the resulting local atmospheric instability becomes larger. Another possible reason on the observation side is the lower conductive heat fluxes $G(i)$ observed in the morning. The lower values of $G(i)$ give higher values of $H(i)$ since the observed sensible heat fluxes were calculated as the residual of $Rn(i) - G(i)$.

In contrast to the sensible heat fluxes, the simulated conductive heat fluxes overestimate the observed values (Figure 8). The heat plates have officially $\pm 5\%$ random error, which cannot account for the bias. The thickness of coating over the heat plate was less than 2 mm, and the heat capacity of the layer negligible. One possible reason for the error above is the three dimensionality of heat conduction in such small-scale concrete cubes. For example, the conductive heat at the roof top will be transferred not only to

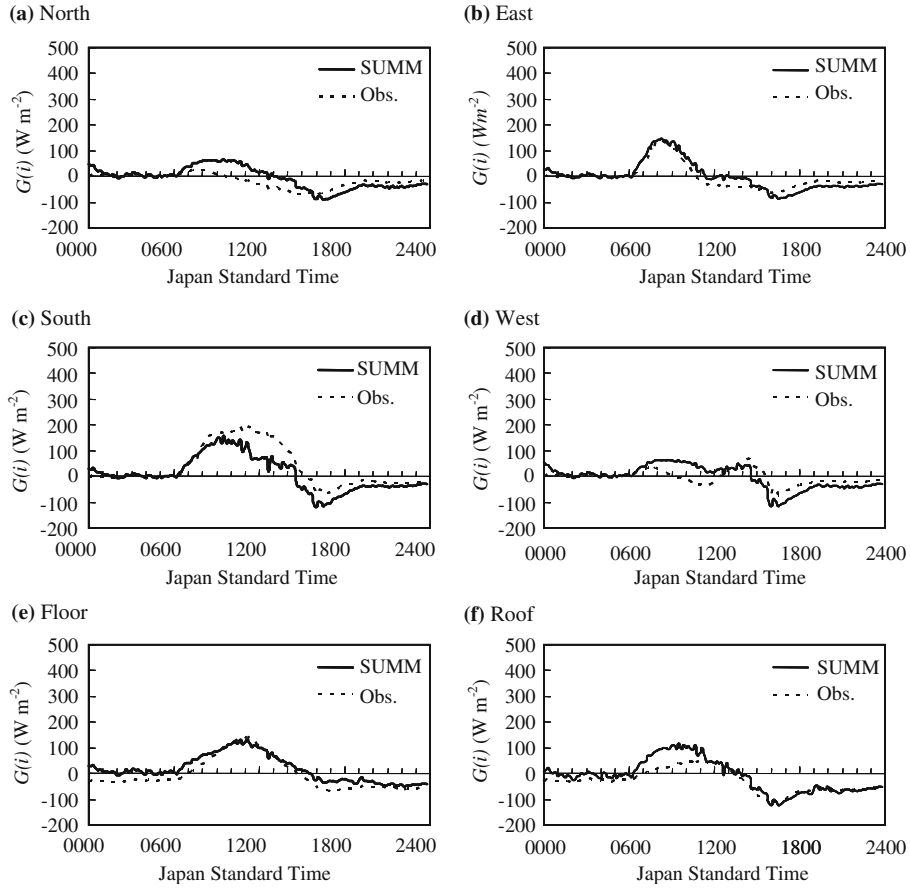

Figure 8. Conductive heat flux in the simulations (bold lines) and measurements (dotted lines).

the vertical direction but also to the adjacent walls. Such three dimensionality of heat conduction within the concrete materials might decrease the measured $G(i)$ at the surface especially in the morning when the temperature inside the cube is still low. The SUMM assumes only vertical heat conduction and no heat exchange between the different constituent surfaces.

The simulated surface temperatures slightly underestimate the observed values (Figure 9). However, the maximum error of the surface temperature is within 3 K, and the diurnal trend is well simulated.

5.2. Energy balance of the surface layer

Although the simulated energy balances and surface temperatures of individual surfaces show some systematic deviations from measured values, the simulated

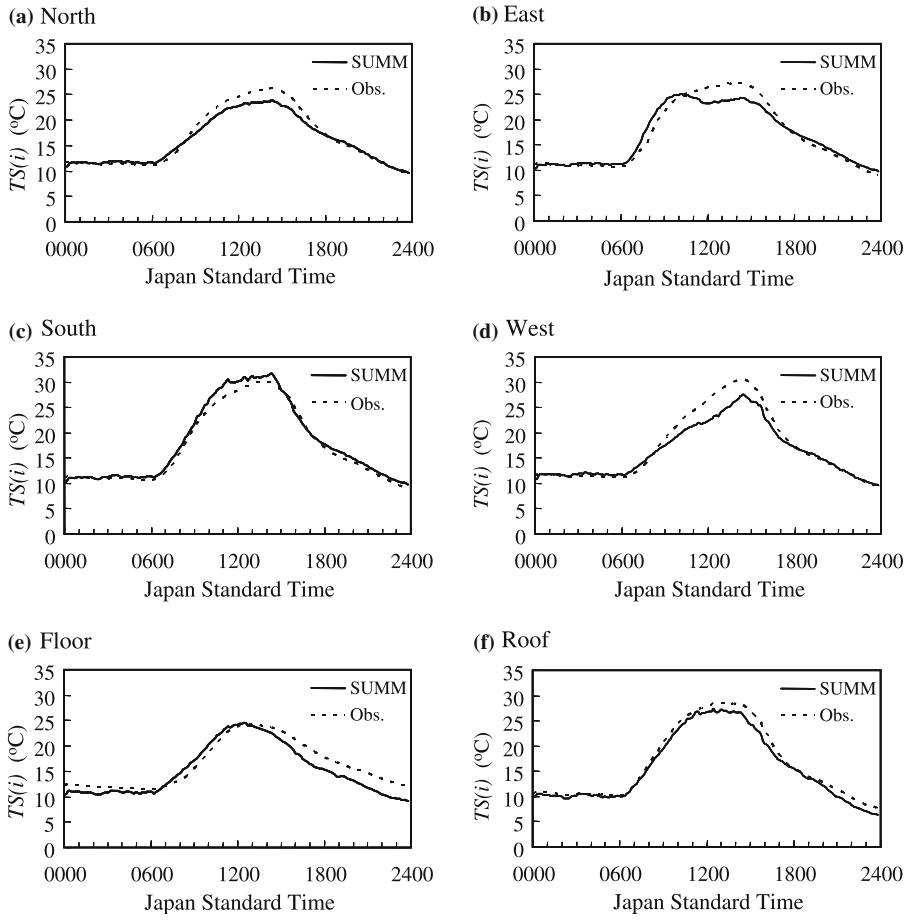

Figure 9. Surface temperature in the simulations (bold lines) and measurements (dotted lines).

energy balance components of the surface layer (*Rn*, *H*, and *G*) agree fairly well with measurements (Figure 10). Probably, the negative and positive biases of heat fluxes of different surfaces cancel when the process is integrated over the canopy layer. This is expected in the present numerical scheme since the 'surface-layer' bulk transfer coefficient is first prescribed from the conventional formulation using roughness parameters and then it is distributed onto individual surfaces. Such top-down parameterisations guarantee compatibility with previous surface-layer parameterisations, although the influence of local stability has not been taken into account. In contrast, bottom-up parameterisations, in which local bulk transfer coefficients are first determined from the local meteorological conditions in the vicinity of surfaces, and then are integrated over the canopy layer, are an alternative approach and more straightforward than the top-down approach (Masson, 2000; Kusaka et al., 2001). In using the bottom-up approach, however, the absolute values of local bulk

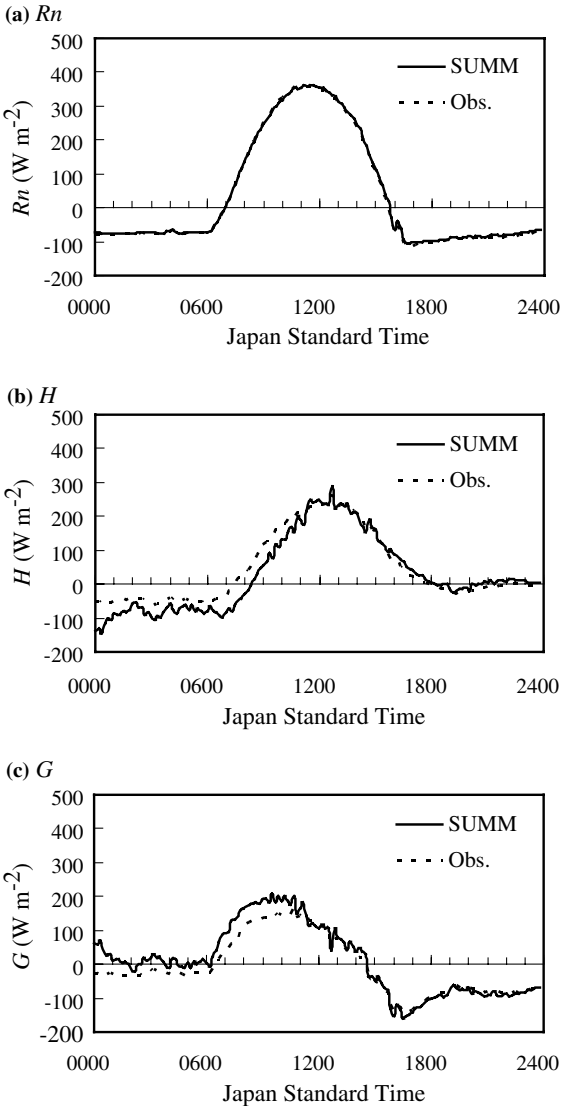

Figure 10. Energy balance components of the surface layer throughout the day. Bold lines are simulation results and dotted lines are measurements. Components are (a) net radiation, (b) sensible heat flux, and (c) conductive heat flux.

transfer coefficients are more crucial, and thus they should be carefully calibrated on site. The review of Hagishima et al. (2005) pointed out that the local bulk transfer coefficients vary considerably from site to site and are currently difficult to determine from a simple formulation, whereas their relative values among individual surfaces are robust, irrespective of measurement site and method, as shown in Figure 5.

5.3. Representative temperatures of the canopy layer

Different representative temperatures of the canopy layer can be derived from the simulation results. We compare three temperatures in Figure 11: the radiative temperature defined by Equation (17), the effective surface temperature defined by Equation (22), and the complete surface temperature, which is the average surface temperature weighted by the constituent surface area (Voogt and Oke, 1997). In the field, the measurement of effective surface temperature is almost impossible, so that it is better to instead use the radiative temperature or the complete surface temperature to estimate the sensible heat flux (Voogt and Grimmond, 2000). The results in Figure 11 show that the effective surface temperature and complete surface temperature are very close and that the radiative temperature is slightly larger than, but can be a good approximation of, the other two. This good agreement is probably due to the openness of the current geometry ($\lambda_p = \lambda_f = 0.25$); the local bulk transfer coefficients and the view factors among the constituent surfaces are relatively close and thus the weighting functions for averaging surface temperatures are similar. Urban canopies with different geometric parameters can produce significant differences among the representative temperatures.

6. Concluding Remarks

A *s*imple *u*rban energy balance *m*odel for *m*esoscale simulations (SUMM) was compared with outdoor scale-model experiments. The following major results were obtained:

(1) The local bulk transfer coefficients for heat of the individual surfaces under neutrally stratified conditions were estimated using the outdoor experiments. The estimated local bulk transfer coefficients normalised by

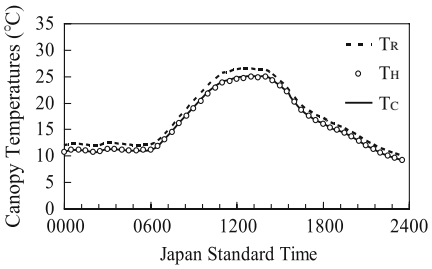

Figure 11. Simulated representative temperatures of the canopy layer. The solid line is the radiative temperature defined in Equation (17), the bold line is the effective surface temperature defined in Equation (22), and the dotted line is the complete surface temperature defined in Voogt and Oke (1997).

the value for the roof surface agreed very well with those obtained from previous indoor experiments.

(2) The SUMM simulated well the observed energy balance of the surface layer. This is because the 'surface-layer' bulk transfer coefficient was first prescribed from the conventional formulation using roughness parameters, and then was distributed into individual surfaces. Such top-down parameterisations in the SUMM guarantee compatibility with previous surface-layer parameterisations.

Recent field studies on urban surface energy indicate that the evaluation of the energy balance at each surface of the urban canopy is important. Moriwaki and Kanda (2004) pointed out that the storage heat flux in the daytime was about the same for summer and winter, irrespective of significant differences in net all-wave radiation, and argued that the abundance of vertical walls can efficiently conserve the energy from radiation even though the solar angle is relatively low. The present model can be used to examine such seasonality in the surface energy balance.

Another possible application of the SUMM is through coupling with a computational fluid dynamical scheme to predict complex turbulent flow within and above the same simple building arrays (e.g. Kanda et al., 2004b).

Acknowledgements

This research was financially supported by Core Research for Evolution Science and Technology of the Japan Science and Technology Cooperation, and by a Grant-in-Aid for Developmental Scientific Research from the Ministry of Education, Science and Culture of Japan.

References

Arnfield, A. J.: 1982, 'An Approach to the Estimation of the Surface Radiative Properties and Radiation Budgets of Cities', *Phys. Geogr.* **3**, 97–122.

Barlow, J. F. and Belcher, S. E.: 2002, 'A Wind Tunnel Model for Quantifying Fluxes in the Urban Boundary Layer', *Boundary-Layer Meteorol.* **104**, 131–150.

Barlow, J. F., Harman, I. N., and Belcher, S. E.: 2004, 'Scalar Fluxes from Urban Street Canyons. Part I: Laboratory Simulation', *Boundary-Layer Meteorol.* **113**, 369–385.

Castro, I. P. and Robins, A. G.: 1977, 'The Flow Around a Surface-mounted Cube in Uniform and Turbulent Streams', *J. Fluid Mech.* **79**, 307–335.

Garratt, J. R.: 1992, *The Atmospheric Boundary Layer*, Cambridge University Press, U.K., 316 pp.

Garratt, J. R. and Francey, R. J.: 1978, 'Bulk Characteristics of Heat Transfer in the Unstable, Baroclinic Atmospheric Boundary Layers', *Boundary-Layer Meteorol.* **15**, 399–421.

Grimmond, C. S. B. and Oke, T. R.: 1999, 'Aerodynamic Properties of Urban Area Derived from Analysis of Surface Form', *J. Appl. Meteorol.* **38**, 1262–1292.

Hagishima, A., Tanimoto, J., and Narita, K.: 2005, 'Review of Experimental Research on the Convective Heat Transfer Coefficient of Urban Surfaces', *Boundary-Layer Meteorol.* In Press.

Kanda, M. and Moriwaki, R.: 2002, 'Surface Parameters in a Densely Built-up Residential Area in Tokyo', *Fourth Symposium Urban Environment*, AMS, Norfolk, U.S.A., pp. 147–148.

Kanda, M., Inagaki, A., Marcus, O. Z., Raasch, S., and Watanabe, T.: 2004a, 'LES Study of The Energy Imbalance Problem with Eddy Covariance Fluxes', *Boundary-Layer Meteorol.* **110**, 381–404.

Kanda, M., Moriwaki, R., and Kasamatsu, F.: 2004b, 'Large Eddy Simulation of Turbulent Organized Structure Within and Above Explicitly Resolved Cube Arrays', *Boundary-Layer Meteorol.* **112**, 343–368.

Kanda, M.: 2005, 'Progress in the Scale Modeling of Urban Climate: Review', *Theor. Appl. Climatol.*, In Press.

Kanda, M., Kawai, T., and Nakagawa, K.: 2005, 'Simple Theoretical Radiation Scheme for Regular Building Array', *Boundary-Layer Meteorol.*, **114**, 71–90.

Kusaka, H., Kondo, H., Kikegawa, Y., and Kimura, F.: 2001, 'A Simple Single-layer Urban Canopy Model for Atmospheric Models: Comparison with Multi-layer and Slab Models', *Boundary-Layer Meteorol.* **101**, 329–358.

Macdonald, R. W., Griffiths, R. F., and Hall, D. J.: 1998, 'An Improved Method for the Estimation of Surface Roughness of Obstacle Arrays', *Atmos. Environ.* **32**, 1857–1864.

Martilli, A., Clappier, A., and Rotach, M. W.: 2002, 'An Urban Surface Exchange Parameterization for Mesoscale Models', *Boundary-Layer Meteorol.* **104**, 261–304.

Masson, V.: 2000, 'A Physically-Based Scheme for the Urban Energy Budget in Atmospheric Models', *Boundary-Layer Meteorol.* **94**, 357–397.

Moriwaki, R. and Kanda, M.: 2003, 'Radiation, Heat, Water-vapor and CO_2 Fluxes in an Urban Surface Layer', *J. Japan Soc. Hydrol. Water Resour.* **16**, 477–490 (in Japanese).

Moriwaki, R. and Kanda, M.: 2004, 'Seasonal and Diurnal Fluxes of Radiation, Heat, Water Vapor and CO_2 over a Suburban Area', *J. Appl. Meteorol.*, **43**, 1700–1710.

Narita, K.: 2003, 'Wind Tunnel Experiment on Convective Transfer Coefficient in Urban Street Canyon', *Fifth International Conference on Urban Climate*, Lodz, Poland, pp. 355–358.

Narita, K.: 2004, 'Effects of Building-Height Heterogeneity on Area-Averaged Transfer Velocity in the Street Surface-Wind Tunnel Experiments Using Salinity Change Technique', *Fifth Symposium on Urban Environment*, AMS, Vancouver, Canada, O6.8.

Rotach, M. W.: 2002, 'Overview on the Basel Urban Boundary Layer Experiment – BUBBLE', *Fourth Symposium on Urban Environment*, AMS, Norfolk, U.S.A., pp. 25–26.

Sailor, D. and Fan, H.: 2002, 'Modeling the Diurnal Variability of Effective Albedo for Cities', *Atmos. Environ.* **36**, 713–725.

Swaid, H.: 1993, 'The Role of Radiative–Convective Interaction in Creating The Microclimate of Urban Street Canyons', *Boundary-Layer Meteorol.* **64**, 231–259.

Uehara, K., Wakamatsu, S., and Ooka, R.: 2003, 'Studies on Critical Reynolds Number Indices for Wind-tunnel Experiments on Flow Within Urban Areas', *Boundary-Layer Meteorol.* **107**, 353–370.

Voogt, J. A. and Oke, T. R.: 1990, 'Validation of an Urban Canyon Radiation Model for Nocturnal Long-wave Fluxes', *Boundary-Layer Meteorol.* **54**, 347–361.

Voogt, J. A. and Oke, T. R.: 1997, 'Complete Urban Surface Temperature', *J. Appl. Meteorol.* **36**, 1117–1132.

Voogt, J. A. and Grimmond, C. S. B.: 2000, 'Modeling Surface Sensible Heat Flux Using Surface Radiative Temperatures in a Simple Urban Area', *J. Appl. Meteorol.* **39**, 1679–1699.